Bulletin de la Société Royale des Sciences de Liège, Vol. 80, 2011, p. 590 - 594

Multi-wavelength diagnostics of massive binary interaction in Eta Carinae

Jose Groh[1*]

[1]Max-Planck-Institut für Radioastronomie, Auf dem Hügel 69, D-53121 Bonn, Germany

Abstract: Eta Car is generally accepted to be a binary system comprised of two massive stars with a total luminosity of $L_{\rm tot} \geq 5 \times 10^6$ L$_\odot$ and total mass of at least 110 M$_\odot$. Most authors agree on a high eccentricity ($e \sim 0.9$) and an orbital period of 2022.7 ± 1.3 days, but light from the companion star has never been unambiguously observed, causing a large uncertainty in the individual masses and in the other orbital parameters such as the orbital inclination and longitude of periastron. We developed two-dimensional radiative transfer models of Eta Car which account for the presence of the low-density cavity and wind-wind interaction zone created by the rarified, fast wind of the companion, as predicted by hydrodynamical simulations. By comparing synthetic line profiles with available observations, we show that the cavity in the dense wind of the primary star strongly affects multi-wavelength diagnostics such as the ultraviolet spectrum, the optical hydrogen lines, and the shape of the near-infrared continuum region. All these diagnostics have been previously interpreted as requiring a latitude-dependent wind generated by a fast-rotating primary star. Ultimately we found that the presence of the companion hampers the determination of the rotational velocity of the primary.

1 Introduction

Eta Carinae is one of the most luminous objects in the Galaxy, and its study provides crucial constraints on massive stellar evolution under extreme conditions. Extensive monitoring of the optical spectrum of Eta Car showed that the spectroscopic events repeat periodically every 5.54 yr (Damineli 1996). This led to the suggestion that Eta Car is a binary system (Damineli et al. 1997) consisting of two very massive stars, $\eta_{\rm A}$ (primary) and $\eta_{\rm B}$ (secondary), with a total system mass amounting to at least 110 M$_\odot$ (Hillier et al. 2001). The spectroscopic events are related to the periastron passage of $\eta_{\rm B}$, and the binary scenario is supported by numerous multi-wavelength observations as summarized by M. Corcoran (2011). Although most orbital parameters of the Eta Car system are uncertain, the wealth of multi-wavelength observations are consistent with a high eccentricity ($e \sim 0.9$) and an orbital period of 2022.7 ± 1.3 d (Damineli et al. 2008).

1.1 Is $\eta_{\rm A}$ a rapid rotator?

$\eta_{\rm A}$ is an LBV star with a high mass-loss rate of $\dot{M} \simeq 10^{-3}{\rm M}_\odot{\rm yr}^{-1}$ and wind terminal velocity of $v_\infty \simeq 500 - 600$ km s^{-1} (Hillier et al. 2001). Based on the variations of Hα absorption line

*email: jgroh@mpifr.de

profiles in scattered light from the Homunculus, which provide us with different viewing directions to the star, and assuming that the rotation axis of $\eta_{\rm A}$ and the Homunculus axis are aligned, Smith et al. (2003) suggested that $\eta_{\rm A}$ has a latitude-dependent wind, with faster, denser outflow in polar directions. Interferometric measurements obtained with VLTI/VINCI (van Boekel et al. 2003; Kervella 2007) and VLTI/AMBER (Weigelt et al. 2007) in the near-infrared K-band continuum are consistent with an ellipsoidal shape projected on the sky, and were interpreted as evidence for a dense prolate wind generated by fast rotation, as theoretically predicted by Owocki et al. (1996). In Groh et al. (2010a) we employed 2-D radiative transfer models of prolate winds generated by rapid rotation to analyze the interferometric observations and obtained that $\eta_{\rm A}$ is spinning at $\sim 80-90\%$ of its critical velocity for break-up. Interestingly, our 2-D models suggest that the rotation axis of the primary star is not aligned with the Homunculus polar axis.

The results described above ignore any possible effects of $\eta_{\rm B}$ on the wind of $\eta_{\rm A}$. However, recent 3-D numerical simulations show that the wind of $\eta_{\rm B}$ significantly influences the geometry of the very dense wind of $\eta_{\rm A}$ via the creation of a cavity and dense wind-wind collision zone (Pittard & Corcoran 2002; Okazaki et al. 2008; Parkin et al. 2009). Here we discuss the influence of $\eta_{\rm B}$ on the optical spectrum and on the geometry of the K-band emission, which are the key diagnostics supporting the fast rotation of $\eta_{\rm A}$.

2 Radiative transfer model

Our models are based on the spherically symmetric models of $\eta_{\rm A}$ (Hillier et al. 2001, 2006), but use the 2-D code of Busche & Hillier (2005) to study the influence of the low-density cavity, and dense interaction-region walls, on the spectrum. Further details are given in Groh et al. (2010a) and Groh et al. (2011, in preparation), and here we outline only the main characteristics of our implementation.

We approximate the cavity as a conical surface with half-opening angle α and interior density 0.0016 times lower than that of the spherical wind model of $\eta_{\rm A}$. We include cone walls of angular thickness $\delta\alpha$ and, assuming mass conservation, a density contrast in the wall of $f_\alpha = [1 - \cos(\alpha)]/[\sin(\alpha)\delta\alpha]$ (Gull et al. 2009) times higher than the wind density of the spherical model of $\eta_{\rm A}$ at a given radius. The conical shape is justified since the observations we model here were taken at orbital phases sufficiently before periastron, when such a cavity has an approximately 2-D axisymmetric conical form (Okazaki et al. 2008). Based on the expected location of the cone apex during these phases (Cantó et al. 1996; Okazaki et al. 2008), we place the cavity at a distance $d_{\rm apex}$ from the primary star. We assume that the material inside the cavity and along the walls has the same ionization structure as the wind of $\eta_{\rm A}$. Thus, at this point we explicitly neglect the ionization changes that might occur in the wind-wind interacting region. We also do not account for the ionizing flux of $\eta_{\rm B}$. Despite these limitations, our implementation should be adequate for understanding how the line profiles of $\eta_{\rm A}$ are modified by the carving of its wind by $\eta_{\rm B}$.

3 Effects of the companion on the optical spectrum of Eta Car

The optical spectrum of Eta Car has been monitored by the Eta Car HST Treasury Project from 1998 to 2004 (Davidson et al. 2005), encompassing slightly more than one orbital cycle. Assuming a single-star scenario with a spherically-symmetric stellar wind, Hillier et al. (2001) obtained a reasonable fit to the observed optical spectrum obtained right after periastron, at orbital phase $\phi \sim 0.05$. The CMFGEN model spectrum from Hillier et al. (2001) reproduced well the emission line profiles of H, Fe II, and N II lines (Fig. 1), yielding the following stellar parameters: stellar temperature $T_\star$ = 35,310 K

(at Rosseland optical depth $\tau_{\rm Ross} = 150$), effective temperature $T_{\rm eff}$= 9,210 K (at $\tau_{\rm Ross} = 2/3$), luminosity $L_\star = 5 \times 10^6$ L$_\odot$, mass-loss rate $\dot{M} = 10^{-3}$ M$_\odot$yr^{-1}, wind terminal velocity $v_\infty = 500$ km s^{-1}, a clumping volume-filling factor $f = 0.1$, and distance $d = 2.3$ kpc.

However, when compared to observations taken at $\phi \sim 0.05$, the spherically-symmetric CMFGEN model overestimates the amount of P-Cygni absorption. The comparison is even worse as one moves toward apastron, when the observations show little or no P-Cygni absorption components in H and Fe II lines (Fig. 1; see also Nielsen et al. 2007). A possible explanation for absence of P-Cygni absorption in the H lines is that the wind of $\eta_{\rm A}$ is latitude dependent (Hillier et al. 2001; Smith et al. 2003).

Using our 2-D radiative transfer model, which takes into account the cavity in the wind of $\eta_{\rm A}$ caused by $\eta_{\rm B}$, we computed the synthetic optical spectrum of Eta Car at $\phi \sim 0.6$ (Fig. 1). We assumed the same parameters described above for $\eta_{\rm A}$ (Hillier et al. 2001) and a standard geometry of the cavity at apastron as predicted by 3-D hydrodynamical simulations (Okazaki et al. 2008; Parkin et al. 2009): $d_{\rm apex} = 19$ AU, $\alpha = 54°$, $\delta\alpha = 3°$ (i.e., $f_\alpha = 9.7$), $b = 0.0016$. For a viewing angle of $i = 41°$ and longitude of periastron of $\omega = 270°$, the 2-D model produces a much better fit to the P-Cygni absorption line profiles of H and Fe II lines than the 1-D CMFGEN model, while still fitting the emission line profiles. The improved fit to the P-Cygni absorption line profiles yielded by the 2-D model is due to the cavity in the wind of $\eta_{\rm A}$, which reduces the H and Fe II optical depths in the line-of-sight to $\eta_{\rm A}$ when the observer looks down the cavity.

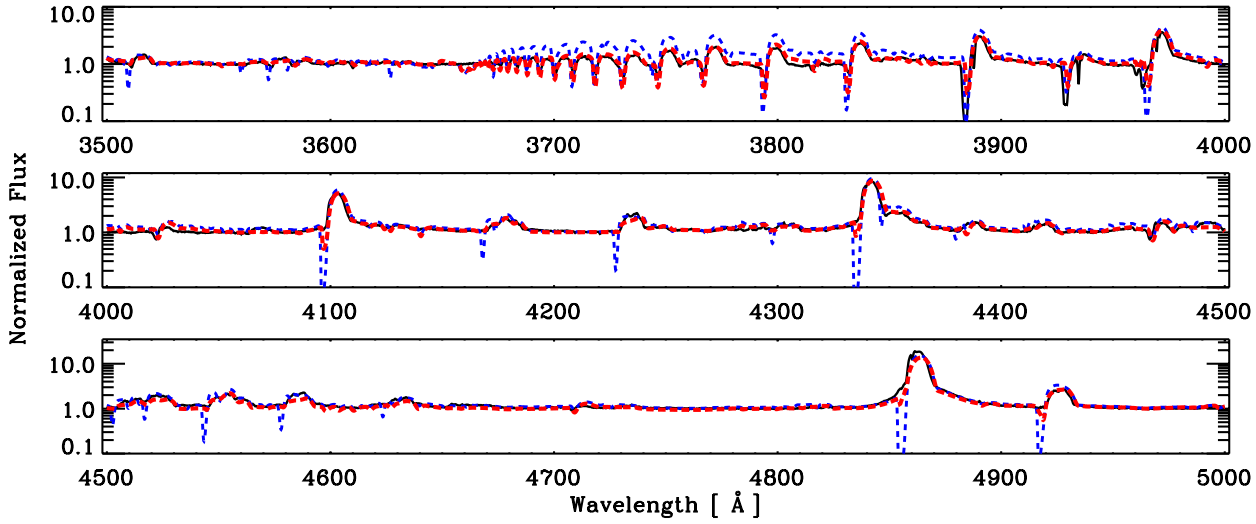

Figure 1: Optical spectrum of $\eta_{\rm A}$ observed with *HST/STIS* at $\phi \sim 0.6$ (solid black line) compared to the spherically-symmetric CMFGEN model from Hillier et al. (2001) (blue dashed line) and with our 2-D model including a cavity and compressed walls created by the wind of $\eta_{\rm B}$ (red dashed line). See text for the model parameters.

4 Effects of the companion on the geometry of the K-band emission

The advent of near-infrared long baseline interferometry has allowed one to spatially resolve the wind of Eta Car using ESO's VLTI/VINCI and VLTI/AMBER instruments (van Boekel et al. 2003; Weigelt et al. 2007). Previously the observations have been interpreted assuming a single-star, latitude-dependent wind generated by rapid rotation. Here we analyze how our 2-D model of the binary

system affects this interpretation. We investigate the influence of $\eta_{\rm B}$ on the inner wind of $\eta_{\rm A}$ through the presence of a low-density cavity and density enhanced wind-wind collision zone, with the goal of determining how these may affect the interpretation of the VLT/VINCI dataset obtained relatively close to periastron. We apply, for the first time for Eta Car, 2-D radiative transfer models with the same parameters as described in Section 3, except for a different orbital phase ($\phi \sim 0.93$).

The amount of influence of the wind-wind interaction on the observables depends on two factors: how close the cavity gets to the K-band emitting region of $\eta_{\rm A}$ ("bore hole effect", Madura & Owocki 2010), and how much free-free radiation is emitted by the dense walls of the shock cone ("wall effect"). According to our models, the main effect from the wind-wind collision zone at the orbital phases analyzed is extended free-free emission from the compressed walls. Such an effect may influence the geometry of the K-band emitting region even at orbital phases far from periastron, depending on the observer's location, geometry of the cavity, i, α, and f_α.

We found that a model with $\alpha = 54°$, $f_\alpha = 9.7$ (i. e., $\delta\alpha = 3°$; Gull et al. 2009), and $i = 41°$ shows significant wall emission and is able to produce a significant elongation of the K-band continuum (Fig. 2). To explain the VLTI/VINCI observations, the symmetry axis of the cavity has to be oriented along PA$\simeq 35° - 45°$ (i.e., SW-NE axis; Fig. 2), which is roughly consistent with that expected from a longitude of periastron of $\omega = 243°$ (e.g., Okazaki et al. 2008; Parkin et al. 2009; Gull et al. 2009, Groh et al. 2010b) and a counterclockwise motion of $\eta_{\rm B}$ on the sky. The $\dot{M}$ of $\eta_{\rm A}$ needs to be slightly reduced to 8×10^{-4} M$_\odot$yr^{-1} to compensate for the extra extension in the K-band emitting region caused by the wall effect.

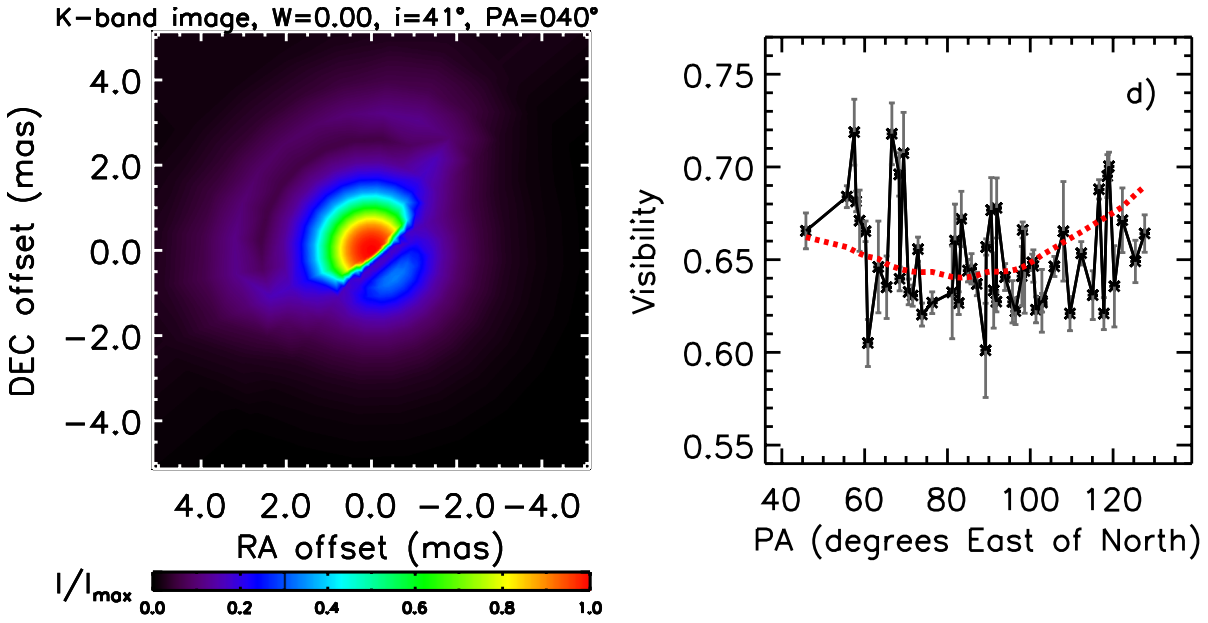

Figure 2: *Left:* Synthetic K-band image predicted by the best-fitting 2-D model of $\eta_{\rm A}$ including a cavity and compressed walls created by the wind of $\eta_{\rm B}$. The model is appropriate for the VINCI observations ($\phi = 0.93$) and assumes $i = 41°$, PA $= 40°$, $d_{\rm apex} = 10$ AU, $\alpha = 54°$, and $\delta\alpha = 3°$. *Right:* Observed VLTI/VINCI visibilities for the 24 m baseline as a function of telescope PA (connected black asterisks) compared to the 2-D cavity model prediction (red dotted line). Note that the projected baseline length of the VINCI measurements changes as a function of PA.

5 Short summary

How much does $\eta_{\rm B}$ affect the H line profiles and the K-band emitting region of $\eta_{\rm A}$, which are the two diagnostics of rapid rotation in $\eta_{\rm A}$? Here we showed that both are *strongly* affected by the presence of $\eta_{\rm B}$, which carves a significant cavity in the wind of $\eta_{\rm A}$. Therefore, an intrinsic latitude-dependent wind produced by fast rotation may not be the only explanation for existing observations, but this does not mean that $\eta_{\rm A}$ is not a rapid rotator. Three-dimensional radiative transfer models will be needed to properly account for both the presence of the cavity and a latitude-dependent wind generated by rapid rotation.

As discussed in Groh et al. (2010a), the presence of the cavity and walls have an effect on the available interferometric observables that is as large as that due to a latitude-dependent wind caused by rapid rotation, although the morphology of the K-band images is noticeably different in the two scenarios. Our 2-D model, in combination with milliarcsecond-resolution images reconstructed from interferometric observations which will be available in the near future, will be the key for probing the effects of the companion and rapid rotation in Eta Car.

Acknowledgements

Many thanks to my collaborators in this project: T. Madura, S. Owocki, J. Hillier, and G. Weigelt. I am grateful to the referee Peredur Williams for the useful comments on the manuscript. I appreciate financial support from the Max-Planck-Society. I would like to congratulate the organizers for putting together a very nice meeting with a fantastic scientific atmosphere. I also appreciate the tasteful prize awarded during the conference dinner, and I think I should thank a *certain* couple of stars for that.

References

Busche, J. R. & Hillier, D. J. 2005, AJ, 129, 454
Cantó, J., Raga, A. C., & Wilkin, F. P. 1996, ApJ, 469, 729
Corcoran, M.F. 2011, in Proceedings of the 39th Liège Astrophysical Colloquium, eds. G. Rauw, M. De Becker, Y. Nazé, J.-M. Vreux & P.M. Williams, BSRSL 80, 578
Damineli, A. 1996, ApJL, 460, L49
Damineli, A., Conti, P. S., & Lopes, D. F. 1997, New Astronomy, 2, 107
Damineli, A., Hillier, D. J., Corcoran, M. F., et al. 2008, MNRAS, 384, 1649
Davidson, K., Martin, J., Humphreys, R. M., et al. 2005, AJ, 129, 900
Groh, J. H., Madura, T. I., Owocki, S. P., Hillier, D. J., & Weigelt, G. 2010a, ApJL, 716, L223
Groh, J. H., Nielsen,K. E. ,Damineli, A., et al. 2010b, A&A, 517, A9
Gull, T. R., Nielsen, K. E., Corcoran, M. F., et al. 2009, MNRAS, 396, 1308
Hillier, D. J., Davidson, K., Ishibashi, K., & Gull, T. 2001, ApJ, 553, 837
Hillier, D. J., Gull, T., Nielsen, K., et al. 2006, ApJ, 642, 1098
Kervella, P. 2007, A&A, 464, 1045
Madura, T. I., & Owocki, S. P. 2010, Rev. Mex. de Astronomia y Astrofisica Conf. Series, 38, 52
Nielsen, K. E., Corcoran, M. F., Gull, T. R., et al. 2007, ApJ, 660, 669
Okazaki, A. T., Owocki, S. P., Russell, C. M. P., & Corcoran, M. F. 2008, MNRAS, 388, L39
Owocki, S. P., Cranmer, S. R., & Gayley, K. G. 1996, ApJL, 472, L115
Parkin, E. R., Pittard, J. M., Corcoran, M. F., Hamaguchi, K., & Stevens, I. R. 2009, MNRAS, 394, 1758
Pittard, J. M. & Corcoran, M. F. 2002, A&A, 383, 636
Smith, N., Davidson, K., Gull, T. R., Ishibashi, K., & Hillier, D. J. 2003, ApJ, 586, 432
van Boekel, R., Kervella, P., Schöller, M., et al. 2003, A&A, 410, L37
Weigelt, G., Kraus, S., Driebe, T., et al. 2007, A&A, 464, 87